Resonant Plasmonic Enhancement of Single-Molecule Fluorescence by Individual Gold Nanorods

Saumyakanti Khatua,[†,⊥] Pedro M. R. Paulo,[‡,⊥] Haifeng Yuan,[†,⊥] Ankur Gupta,[†] Peter Zijlstra,[§] and Michel Orrit[†,*]

[†]Huygens-Kamerlingh Onnes Laboratory, Universiteit Leiden, 2300 RA Leiden, The Netherlands, [‡]Centro de Química Estrutural, Instituto Superior Técnico, Universidade de Lisboa, Avenida Rovisco Pais 1, 1049-001 Lisboa, Portugal, and [§]Department of Applied Physics, Eindhoven University of Technology, 5612 AZ Eindhoven, The Netherlands. [⊥]S. Khatua, P. M. R. Paulo, and H. Yuan contributed equally.

ABSTRACT Enhancing the fluorescence of a weak emitter is important to further extend the reach of single-molecule fluorescence imaging to many unexplored systems. Here we study fluorescence enhancement by isolated gold nanorods and explore the role of the surface plasmon resonance (SPR) on the observed enhancements. Gold nanorods can be cheaply synthesized in large volumes, yet we find similar fluorescence enhancements as literature reports on lithographically fabricated nanoparticle assemblies. The fluorescence of a weak emitter, crystal violet, can be enhanced more than 1000-fold by a single nanorod with its SPR at 629 nm excited at 633 nm. This strong enhancement results from both an excitation rate enhancement of ~130 and an effective emission enhancement of ~9. The fluorescence enhancement, however, decreases sharply when the SPR wavelength moves away from the excitation laser wavelength or when the SPR has only a partial overlap with the emission spectrum of the fluorophore. The reported measurements of fluorescence enhancement by 11 nanorods with varying SPR wavelengths are consistent with numerical simulations.

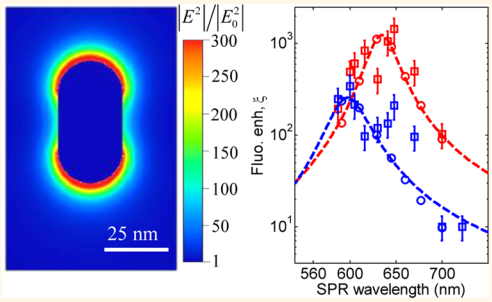

KEYWORDS: plasmon-enhanced fluorescence · gold nanorods · single-molecule fluorescence · surface plasmon resonance

Since its discovery in the early 1990s, single-molecule imaging and spectroscopy has seen a tremendous growth and has established itself as an important tool for studying many complex systems in chemistry, biology, and physics owing to its unique access to the nanometer scale.[1] New information has emerged about dynamic heterogeneities in supercooled liquids,[2,3] subwavelength arrangement of cell components,[4] and dynamics of proteins and enzymes.[5,6] Currently, single-molecule spectroscopy mostly relies on fluorescence, as it provides fast, high-contrast, and low-background detection of single molecules. The key requirement of this technique is that the molecules under investigation must have a sufficiently high photon emission rate. However, a large fraction of strongly absorbing molecules, including many biologically relevant proteins and metal complexes, fluoresce only weakly. This weak emission is due to a low fluorescence quantum yield or a long fluorescence lifetime, rendering these species undetectable by single-molecule spectroscopy. Enhancing the fluorescence rate of such weak emitters will expand the reach of single-molecule spectroscopy into new and yet unexplored territories.

Plasmonic nanostructures are known to enhance the rate of fluorescence of weak emitters.[7−9] Such enhancements originate from two factors. A plasmonic nanoparticle can act as an antenna and confine the electromagnetic field of incident light into a tiny volume near its surface. This concentrated field leads to an increase in absorption of light by a molecule when placed in the vicinity of the nanoparticle and corresponds to an excitation enhancement, E_{exc}. The nanoparticle antenna may also enhance fluorescence by altering the radiative and nonradiative decay rates of a molecule, leading to an effective emission enhancement, E_{em}. This quantity involves the emitter's photophysics, and we define it through the experimentally observed overall fluorescence

* Address correspondence to orrit@physics.leidenuniv.nl.

Received for review December 16, 2013 and accepted March 31, 2014.

Published online March 31, 2014
10.1021/nn406434y

enhancement ξ, by the relation $\xi = E_{exc} \times E_{em}$. These different enhancement factors generally depend on the local field induced by the nanoparticle, on the position and orientation of the molecule relative to the nanoparticle, and on the extent of spectral overlap between the molecule and the nanoparticle.[10] Fluorescence can also be quenched by the nanoparticle when the molecule is too close to the metal.[11,12] This phenomenon, which can be seen as a Förster energy transfer process, can also be explained by coupling to higher order dark modes, which decay faster than the dipolar mode.[12,13]

Fluorescence enhancement by plasmonic nanoparticles has been studied extensively over the past few decades. Early reports by the groups of Sandoghdar[14] and Novotny[15] employed a single gold nanosphere of 80 nm in diameter and achieved a fluorescence enhancement of a factor of 9. The fluorescence enhancement near gold nanospheres is modest because of the relatively small field enhancement (~5 times). Much effort has been spent to prepare nanostructures that generate higher fluorescence enhancements. For example, bowtie nanoantennas consisting of two triangular nanoparticles with a small gap were used by the groups of Moerner[16] and Hecht[17] and provide fluorescence enhancements of up to 1300 for weak emitters.[16] More recent examples include directional Yagi-Uda and corrugated nanoantennas by the groups of Van Hulst[18] and Wenger.[19] These nanoantennas consist of assemblies of two or more nanostructures with narrow gaps between them to achieve the necessary fluorescence enhancement. They are therefore fabricated by lithographic methods that are expensive and do not easily allow for the fabrication of large numbers of antennas. Moreover, lithographic nanostructures exhibit broad plasmon resonances because they are polycrystalline, and they are grown on a chromium or titanium wetting layer.[20]

Here we show that isolated gold nanorods provide fluorescence enhancements similar to lithographic assemblies. They do not require a carefully controlled nanogap to achieve >1000-fold enhancement because the single-crystalline nature of the particles results in a narrow plasmon resonance and a high local field.[21] Moreover, they are easily produced in large numbers using wet-chemical methods that only require basic chemical lab equipment.[22,23] Their flexible surface chemistry using thiolated ligands makes them compatible with a broad range of solvents and would enable the future prospect of using them, for example, within live cells.[24,25] Fluorescence enhancements of up to several thousands have been predicted theoretically[26,27] and were experimentally demonstrated recently.

In this article, we demonstrate the crucial role of the SPR in gold nanorods toward enhancing single-molecule fluorescence, both theoretically and experimentally. We show that the fluorescence enhancement indeed strongly depends on the nanorod SPR wavelength and is maximum when both the excitation laser and the dye's emission spectrum overlap with the SPR. The optimum SPR wavelength generates a fluorescence enhancement of 1100, consisting of an excitation rate enhancement of about 130-fold and an effective emission enhancement of about 9-fold. This is in good agreement with numerical calculations based on the discrete dipole approximation.

RESULTS AND DISCUSSIONS

We define the transition rates of a molecule in a vacuum and in the presence of a nanoantenna according to Scheme 1. The excitation, radiative decay, and nonradiative decay rates of the molecule in a vacuum are given as σI, k_r, and k_{nr}, respectively (σ is the dye's absorption cross section at the excitation wavelength and I is the excitation laser intensity). In the vicinity of the antenna, the local electric field leads to modifications of the excitation rate and of the emission rate. Because we suppose excitation is done with a laser at a well-defined wavelength, the excitation enhancement E_{exc} is purely electromagnetic and depends only on the laser wavelength. Fluorescence emission, however, involves many different spectral components λ, each of which will present its own radiative enhancement $E_{rad}(\lambda)$. The electromagnetic enhancement of the emission rate, E_r, results from averaging over all spectral components of the fluorescence:

$$E_r = \int E_{rad}(\lambda)\, F(\lambda)\, d\lambda \qquad (1)$$

where $F(\lambda)$ is the normalized fluorescence spectrum of the dye. Similarly, the additional nonradiative decay K_{nr} induced by the antenna also results from a sum over all spectral components of the fluorescence. In the following, we discuss radiative and nonradiative decay at a single wavelength and perform the averaging at the end, before comparing to experiments.

On the basis of this simple scheme, we define the overall fluorescence enhancement factor (ξ) induced by a nanoantenna as the ratio of emitted intensities with and without an antenna. For fluorescence at a single wavelength (only one spectral component),

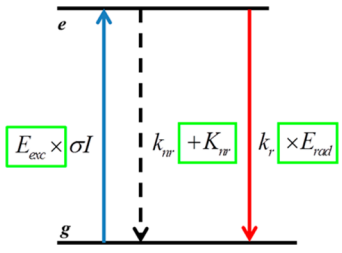

Scheme 1. Simple two-level scheme describing the transition rates of a molecule without and with (changes highlighted in green boxes) a gold nanorod antenna. σ is the absorption cross section of the molecule, and I is the excitation laser intensity.

we find (see Supporting Information for more details)

$$\xi = E_{exc}E_{rad}\frac{\sigma I + k_{nr} + k_r}{E_{exc}\sigma I + k_{nr} + K_{nr} + E_{rad}k_r} \quad (2)$$

Under weak enough excitation ($E_{exc}\,\sigma I \ll k_{nr} + K_{nr} + E_{rad}k_r$) eq 2 can be simplified to

$$\xi \approx E_{exc}E_{rad}\frac{k_{nr} + k_r}{k_{nr} + K_{nr} + E_{rad}k_r} \quad (3)$$

For the limiting case where $E_{rad}k_r \ll k_{nr}$ and $K_{nr} \ll k_{nr}$, *i.e.*, for dyes with very low fluorescence yield ($\eta \ll 1$), one can further simplify eq 3 to a commonly used form:[26]

$$\xi \approx E_{exc} \times E_{rad}$$

To keep our discussion valid for a broad range of dyes, we use eq 3 in the rest of this paper, because it applies to any dye as long as the (enhanced) excitation intensity is well below saturation (see Supporting Information).

To theoretically estimate the ξ values according to eq 3, one needs the intrinsic decay rates of the dye (k_r and k_{nr}), the excitation and radiative decay rate enhancement factors (E_{exc} and E_{rad}), and the additional nonradiative rate (K_{nr}). The intrinsic decay rates of the dye are calculated from the measured QY and the florescence lifetime. For crystal violet (CV) molecules, k_r and k_{nr} are estimated to be 1.9×10^7 s^{-1} and 9.8×10^8 s^{-1} based on the measured QY of 0.02[28] and the fluorescence lifetime of 1 ns.

E_{exc}, E_{rad}, and K_{nr} are purely electromagnetic in nature and can be theoretically calculated using a classical electrodynamics description that models the molecule as a radiating point dipole in the vicinity of a metal surface. For particles with complex geometries, the solution of this Maxwell problem is calculated from a suitable numerical method, such as finite difference time domain (FDTD), discrete dipole approximation (DDA), or finite-element method (FEM). In this work, we have used the DDA method to evaluate the enhancement in the excitation, radiative, and nonradiative rates of a CV molecule close to a gold nanorod. The nanorod's shape is a spherically capped cylinder. The nanorod is described as an array of dipoles replacing cubic volume elements, 0.25 nm in size. The size of the dipole elements was chosen to get the best compromise between computational time and accuracy of the calculated results. The latter could still be improved by reducing the dipole size, *e.g.*, to a size of 1/16 nm, but at the cost of significantly increasing computational time without further insight being attained. The calculations use the dielectric function of gold, as reported by Johnson and Christy.[29]

As the excitation rate enhancement E_{exc} we took the ratio of local field intensities with and without antenna, $E_{exc} = |\mathbf{E}(\mathbf{r}_0)|^2/|\mathbf{E}_0(\mathbf{r}_0)|^2$, at the molecule's position $\mathbf{r}_0$. We assume that the particle is excited by a plane wave polarized along the long axis of the rod. The enhancement of the radiative rate E_{rad} and the additional nonradiative rate K_{nr} were calculated following the approach of D'Agostino *et al.*[30] The new implementation of DDA by D'Agostino *et al.* allows one to introduce an arbitrary user-defined excitation source. In the calculation of E_{rad} and K_{nr}, it was assumed that the excitation source was a point-like dipole with the emission characteristics of a CV molecule, *i.e.*, a transition dipole moment of $|\mathbf{p}_0|$ = 6.6 D. The point source dipole from the emitting molecule was calculated on the set of coordinates that discretize the particle using the classical expression for the electric dipole field.[31] It was assumed that the transition dipole moment of the molecule is oriented along the long axis of the rod and that the molecule is placed on the revolution axis of the rod, which provides the largest enhancements. This is obviously not always the case in the experiments, but comparison with the theoretical results still holds, because it is based on the largest effects experimentally observed.

The enhancement of the radiative rate E_{rad} is derived by assuming the molecule−nanoparticle system is so small that it behaves as a single effective point dipole, formed from the particle's induced dipole $\mathbf{p}_{ind}$ and that of the molecule itself:

$$E_{rad} = \frac{|\mathbf{p}_{ind} + \mathbf{p}_0|^2}{|\mathbf{p}_0|^2} \quad (4)$$

where $\mathbf{p}_{ind} = \sum_{i=1}^{N}\mathbf{p}_i$ is the sum of the polarization elements $\mathbf{p}_i$, *i.e.*, the polarization calculated from DDA on the *i*th dipolar element. Obviously, this approximation is valid only for small nanoparticles and small molecule−nanoparticle distances.

The additional nonradiative rate is derived from the time-averaged power absorbed by the metal nanoparticle:[30]

$$K_{nr} = \frac{P_{abs}}{\hbar\omega} \approx \frac{\varepsilon_0}{2\hbar}\mathrm{Im}(\varepsilon)\left[\sum_{i=1}^{N}|\mathbf{E}_{local,i}|^2 \times V_c\right] \quad (5)$$

where ε is the complex dielectric permittivity of gold at the emitted frequency; $\mathbf{E}_{local,i}$ is the internal electric field calculated at the position of the *i*th dipole element, which has the contribution from a incident field, plus the field due to all other dipoles; and V_c is the volume of each dipole element. The separation between the emitter and the particle surface was varied between 1 and 20 nm to evaluate the distance effect on the rate enhancements. We note that a classical description is valid throughout this range of distances, as significant quantum effects are expected only at distances less than 1 nm.[32]

The near-field intensity maps of seven individual gold nanorods with their SPRs ranging from 560 to 700 nm were calculated at excitation wavelengths of 594 and 633 nm using the DDA method. The SPR wavelengths are varied by tuning the nanorod length

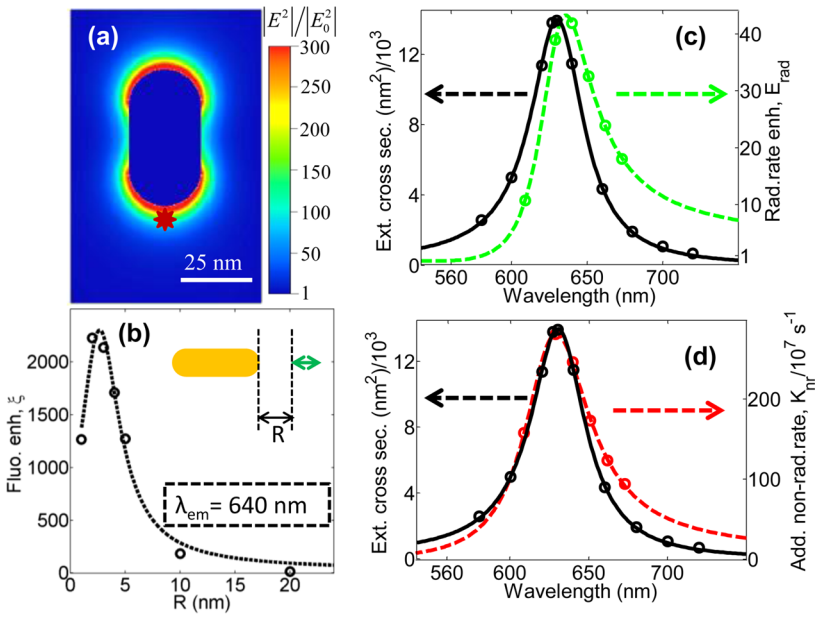

Figure 1. (a) Calculated near-field intensity map of a gold nanorod that is 47 nm long and 25 nm wide. The SPR of the nanorod is located at 629 nm. The excitation wavelength is 633 nm, and the excitation is polarized along the long axis of the nanorod. (b) Calculated overall fluorescence enhancement factor (ξ, open circles) at an emission wavelength of 640 nm as a function of distance (R) between the nanorod and the CV molecule. In panels (c) and (d), the distance between the CV molecule and the tip of the rod is fixed to 5 nm. (c) Calculated radiative rate enhancement (E_{rad}) of a CV molecule as a function of emission wavelength (green circles). (d) Additional nonradiative rate (K_{nr}) as a function of emission wavelength (red circles). The extinction spectrum of the nanorod is shown by the black circles in (c) and (d). A skewed Lorenzian fit to the extinction spectrum is shown as the black solid lines in (c) and (d). For (b), (c), and (d) the dipole of the CV molecule is assumed to be oriented parallel to the nanorod dipole, to model the maximum enhancement. The dashed lines in (b), (c), and (d) are guides for the eye. $k_r = 1.9 \times 10^7\ s^{-1}$ and $k_{nr} = 9.8 \times 10^8\ s^{-1}$.

from 39 to 60 nm while keeping a constant diameter of 25 nm. Figure 1a shows the near-field intensity map of a 25 nm × 47 nm gold nanorod (SPR 629 nm) at 633 nm excitation. The near-field intensity maps of the other nanorods are shown in the Supporting Information (Figure S1). The near-field intensity maps show that the intensity enhancement is maximum for the nanorod whose SPR matches the excitation laser. For 633 nm excitation, a maximum intensity enhancement by a factor of several hundred is achieved by a nanorod with its SPR at 629 nm (Figure 1a). For the same excitation wavelength, a nanorod that has an SPR at 700 nm shows a much weaker intensity enhancement (less than 10).

To calculate the overall fluorescence enhancements (ξ) by a nanorod with a given SPR, we first determine the optimum distance between a CV molecule and the nanorod where ξ is maximum. Our results are shown in Figure 1b which shows ξ as a function of distance between a CV molecule and a nanorod (25 nm × 47 nm). For simplicity, we monitored the radiative rate enhancement (E_{rad}) and the additional nonradiative rate (K_{nr}) at a single wavelength of 640 nm, which corresponds to the maximum of the emission spectrum of CV. From Figure 1b, we clearly identify two distinct regions of space around a nanorod where either the fluorescence enhancement or the quenching dominates. CV fluorescence monotonically increases when the distance between CV and the nanorod's tip decreases until a minimum distance of 3 nm. For shorter distances, however, fluorescence quenching becomes dominant and the overall enhancement decreases again. This trend of ξ *versus* dye−nanorod distance is also seen for all the other nanorods (Figure S2). For all further calculations a fixed dye−nanorod distance of 5 nm was used. This distance roughly is the one at which the enhancement has decayed to half its maximum value (going away from the rod) and gives us an average enhancement somewhat lower than the absolute maximum.

For each nanorod, we calculate the radiative rate enhancement factor (E_{rad}) and the additional nonradiative decay rate (K_{nr}) at different emission wavelengths for an emitting dipole located at a fixed distance of 5 nm from the nanorod's tip. The results of these calculations on a nanorod with SPR at 629 nm are shown in Figure 1c (E_{rad}, green circles) and Figure 1d (K_{nr}, red circles). As shown by Figure 1c,d, both E_{rad} and K_{nr} strongly depend on the emission wavelength, and both of them reach their respective maxima near the SPR of the nanorod. There are, however, two important differences between the wavelength dependence of E_{rad} and the extinction spectrum of the nanorod. First, E_{rad} shows a maximum at a wavelength that is slightly red-shifted (~10 nm) compared to the SPR of the nanorod.

Second, E_{rad} has a markedly asymmetric line shape compared to the Lorentzian SPR line shape (black line in Figure 1c).

This difference between SPR absorption and enhancement spectra has been reported by other authors. It resembles the difference between near-field and far-field intensity spectra, as visualized in Figure S3. Different physical mechanisms have been proposed to explain this difference. A first possible cause is damping, which, as is well known from classical mechanics, causes a resonance shift.[33] A second cause of deviation is that the near field responsible for enhancement is dephased compared to the far field.[34] A third effect arises from the phase difference between the molecule's dipole and the driven SPR dipole. On the red wing of the SPR, the molecular and nanorod dipoles are in phase, but they are dephased by $\pi/2$ at the resonance. These three mechanisms probably contribute to the observed shift.

As noted above, different spectral components of the emission spectrum of CV (Figure 3) will be enhanced by different amounts, corresponding to different E_{rad} values, according to their overlap with the SPR (fwhm ~100 meV). The same applies to the additional nonradiative rate K_{nr}. Therefore, the full enhancement for each spectral component should be calculated according to eq 3 and the results averaged according to eq 1. Instead, we shall do the approximation of an average radiative rate enhancement and of an average additional nonradiative rate to be included in eq 3. This approximation allows us to give average numbers for the enhancement factors and for the additional nonradiative rates. We checked that it does not change our results by more than 20%. Averaging over the entire emission spectrum of CV, we obtain

$$E_r \approx \int E_{rad}(\lambda) \times F_{CV}(\lambda)\, d\lambda,$$

$$K_{nr} \approx \int K_{nr}(\lambda) \times F_{CV}(\lambda)\, d\lambda \qquad (6)$$

where $F_{CV}(\lambda)$ represents the normalized fluorescence spectrum of CV ($\int F_{CV}(\lambda)\, d\lambda = 1$). The overall fluorescence enhancement then becomes

$$\xi \approx E_{exc} E_r \frac{k_{nr} + k_r}{k_{nr} + K_{nr} + E_r k_r} \qquad (7)$$

We can rewrite eq 7 in the form $\xi = E_{exc} \times E_{em}$, defining E_{em} as the effective emission enhancement factor. This factor depends on the radiative decay rate enhancement and the additional nonradiative decay rates due to the presence of the antenna, but also on the photophysical properties of the dye. The excitation enhancement factor E_{exc}, however, is purely electromagnetic and does not depend on the dye.

Finally, we calculate E_r, K_{nr}, E_{em}, and ξ for each nanorod considering the emission wavelength dependence of $E_{rad}(\lambda)$ and $K_{nr}(\lambda)$ (see Figure S4) as discussed

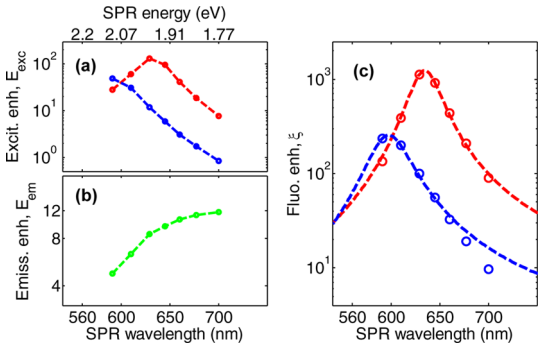

Figure 2. (a) Calculated excitation rate enhancement (E_{exc}) for seven gold nanorods plotted as a function of the SPR wavelength. The excitation wavelengths are 594 nm (blue) and 633 nm (red). (b) Effective emission enhancement factors (E_{em}) of the same nanorods plotted as functions of their SPR wavelengths. (c) Overall fluorescence enhancements (ξ) as functions of the SPR wavelength. Excitation wavelengths are 594 nm (blue) and 633 nm (red). The distance between the molecule and the nanorod's tip was 5 nm.

previously. The wavelength range was selected to account for the broad emission spectrum of CV (Figure 3c). Our results are shown in Figure 2 (see Table 1 in the Supporting Information for details). As expected, for a given excitation wavelength, the excitation enhancement factor (Figure 2a) strongly depends on the SPR wavelength and is maximum for excitation at the SPR wavelength. The effective emission enhancement (E_{em}) for CV molecules, on the other hand, shows a different trend with the SPR wavelength (Figure 2b). E_{em} values are higher for longer wavelengths and increase monotonically until ~700 nm.

The overall fluorescence enhancement factors (ξ) for two excitation wavelengths of 594 nm (blue) and 633 nm (red) are shown in Figure 2c. First, we note that fluorescence enhancements in excess of 1000-fold can be achieved by using a gold nanorod. Figure 2c predicts a maximum fluorescence enhancement of 1100-fold by a nanorod with SPR of 629 nm using 633 nm excitation. This strong enhancement is a combination of an excitation rate enhancement (E_{exc}) of 130 and an effective emission enhancement (E_{em}) of 8.6. These numbers clearly show that in the presence of the antenna not only is a molecule excited with enhanced intensity, but its radiative rate is enhanced as well. As the nonradiative rate is also increased, the fluorescence lifetime will be shortened. Second, we observed that the fluorescence enhancement is maximum when the nanorod's SPR matches the excitation wavelength. For 633 nm excitation, a nanorod with SPR at 700 nm shows a ξ value of only 90 compared to the ξ value of 1100 for a nanorod with SPR at 629 nm. For 594 nm excitation, the maximum fluorescence enhancement is achieved by using a nanorod with SPR at 591 nm. The maximum enhancement, however, is only 225-fold, which is approximately 5 times smaller than the maximum enhancement observed with 633 nm

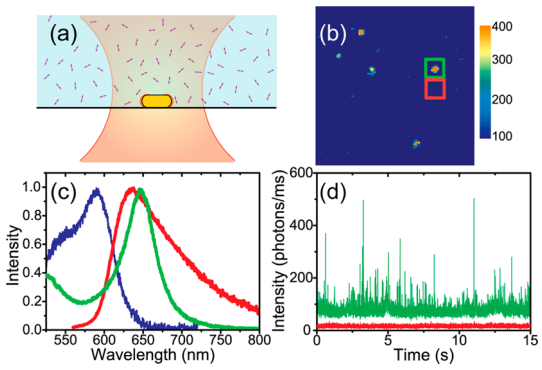

Figure 3. (a) Simple schematics of our experiment (double-headed arrows represent CV molecules; the yellow cylinder, a gold nanorod). (b) Typical one-photon-photoluminescence image of individual gold nanorods covered with a 50 nM CV solution in glycerol. Excitation at 633 nm, acquisition rate 10 ms/pixel. (c) Green line: One-photon-excited luminescence spectrum of the gold nanorod highlighted with a green box in Figure 1b, excited at 514 nm. Blue and red curves show the absorption and fluorescence spectra of CV in glycerol. (d) Green trace: Fluorescence time trace recorded on the same gold nanorod. Red: Background fluorescence with no nanorod present.

excitation. This smaller enhancement results mainly from the lower effective emission enhancement (E_{em}) for an SPR at 591 nm due to the poor spectral overlap with the fluorescence spectrum of CV (maximum at 640 nm), but other factors such as interband transitions and a weaker lightning rod effect probably contribute too.

We performed fluorescence enhancement experiments on CV molecules in the vicinity of individual gold nanorods with their SPRs ranging from 560 to 720 nm. Gold nanorods were immobilized on a glass surface and covered with a 50 nM solution of CV in glycerol (Figure 3a). Figure 3b shows a typical one-photon-excited luminescence image of individual gold nanorods. A circularly polarized 633 nm laser was used as the excitation source. The bright spots in Figure 3b correspond to the photoluminescence signal originating from single gold nanorods. This was checked on all spots studied by measuring the full photoluminescence spectrum of each one under 514 nm laser excitation. The photoluminescence spectrum of the gold nanorod highlighted in the green box in Figure 3b is shown in Figure 3c as a typical example. Narrow and Lorentzian line shapes confirm that the spots arise from single gold nanorods.[35] Aggregates of nanorods usually produce broad non-Lorentzian spectra, often with more than one longitudinal peak or with a plasmon resonance well shifted from the expected resonance position of a single nanorod.[36,37]

Figure 3d shows a fluorescence time trace recorded on the single gold nanorod highlighted in Figure 3c excited with a circularly polarized 633 nm laser. The fluorescence time trace shows bursts that are due to the enhanced fluorescence from the CV molecules passing close to the tips, through the near-field volume of the nanorod. We checked that these bursts are absent in the absence of CV molecules (Figure S7) and in fluorescence time traces measured at places where no nanorod was present (red line in Figure 3d). Moreover, the fluorescence intensity bursts are predominantly polarized along the long axis of the nanorod (Figure S8), confirming that the enhancement is induced by the longitudinal surface plasmon of the nanorod. It is important to note that fluorescence bursts are also seen in a typical fluorescence correlation spectroscopy (FCS) measurement when single molecules enter and leave the focal volume of the laser. However, this is not the case in our experiment. At the CV concentration used here, there are ~30 molecules already present in the focal volume at a given time. Addition of one more molecule into the focal volume cannot cause the dramatic changes in intensity seen in Figure 3d.

We can determine the maximum fluorescence enhancement factor from the enhanced fluorescence signal from a CV molecule, *i.e.*, the strongest fluorescence burst from the time trace in Figure 1d (see Figure 4 for a more quantitative determination) and from the fluorescence count rate from an unenhanced CV molecule. Fluorescence signals from individual unenhanced CV molecules can be calculated from the time trace taken at a place where no nanorod was present. Figure 3d shows such a time trace with an average intensity of 12.1 ± 4.2 counts/ms, resulting from approximately 30 molecules present in the focal volume of the excitation laser. This leads to an average fluorescence signal of 0.4 ± 0.1 count/ms from a single unenhanced CV molecule. The maximum intensity of the fluorescence burst shown in Figure 3d is 502 counts/ms, corresponding to an increase of 422 counts/ms over the background signal of 80 counts/ms (which includes fluorescence from unenhanced CV molecules and luminescence from the nanorod). This increase is due to the enhanced fluorescence from one single CV molecule passing through the near field of the nanorod. As each unenhanced CV molecule produces ~0.4 ± 0.1 count/ms, this burst leads to a calculated fluorescence enhancement factor of 1050 ± 200. We can rule out the possibility that the strongest bursts are caused by more than one CV molecule because at the given concentration of 50 nM, less than 0.001 CV molecules are present in the near field of the nanorod (~10^4 nm^3). Therefore, the probability to have two molecules, 10^{-6}, is negligible. Note that this experimentally determined enhancement factor of 1050 ± 200 is very close to our theoretically predicted enhancement factor of 920 at 5 nm distance for a nanorod with an SPR at 645 nm.

More information regarding these fluorescence bursts can be obtained from the autocorrelation analysis of the fluorescence time traces. Figure S9 shows a typical autocorrelation curve. A single-exponential fit to the autocorrelation trace yields a correlation time of 124 ms. This time corresponds to the average width of

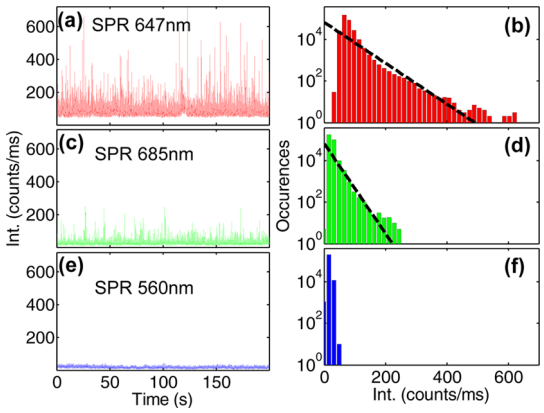

Figure 4. (a, c, e) Fluorescence time traces recorded on three nanorods with SPRs at 647, 685, and 560 nm. Excitation wavelength 633 nm, acquisition time 1 ms. (b, d, f) Intensity histograms constructed from the traces in (a, c, e). The dashed lines in (b) and (d) are fits by exponentially decaying probability distributions.

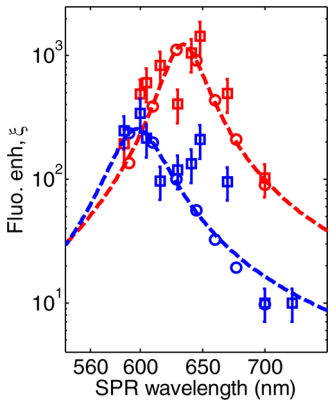

Figure 5. Measured maximum fluorescence enhancement factors for 11 nanorods as functions of their SPR wavelengths under 594 nm (blue squares) and 633 nm (red squares) excitation. The theoretically estimated enhancement factors are shown as open circles (red: 633 nm, blue: 594 nm excitation). Dotted lines are guides to the eye.

the fluorescence burst and hence the average time that individual CV molecules spend in the plasmonic near field of the nanorod before bleaching. On the basis of the bulk viscosity of glycerol, we estimate the diffusion time of a single CV molecule in the near-field of a gold nanorod (~30 nm in average size) to be a few milliseconds. The measured correlation time is therefore significantly longer than the expected diffusion time. We speculate that this longer time is due to sticking of the CV molecules onto the substrate in the vicinity of the rod's tip, followed by photobleaching. This sticking−bleaching mechanism results in fluorescence bursts whose width should depend on the excitation laser intensity. Similar instances of fluorophores binding to the surface near a bowtie nanoantenna were also reported by Kinkhabwala *et al.*[38] Note that sticking of CV molecules to the gold surface would result in complete quenching of their fluorescence and hence is not expected to influence the fluorescence bursts. The interplay between diffusion and sticking−bleaching dynamics will be studied separately in a forthcoming publication.

To experimentally demonstrate the role of the surface plasmon of gold nanorods on the observed fluorescence enhancement, we repeated the fluorescence enhancement experiment on a few nanorods with SPR wavelengths ranging from 570 to 720 nm. In Figure 4, we show fluorescence time traces (a, c, e) recorded on three nanorods with SPRs at 647, 685, and 560 nm under identical experimental conditions. The time traces clearly show that the fluorescence burst intensities strongly depend on the nanorod SPR wavelength. The nanorod with an SPR at 647 nm shows very strong fluorescence bursts (Figure 4a), whereas no significant burst was observed for the nanorod with an SPR at 560 nm (Figure 4e). Visible but significantly weaker bursts are observed for the nanorod with its SPR at 685 nm (Figure 4c). The same trend was also observed in the corresponding intensity histograms shown in Figure 4b,d,f. Figure 4b shows a very broad distribution of intensities with a significant population of high-intensity bursts with average intensities as high as 600 counts/ms. The probability of such high-intensity bursts clearly decreases for the other two nanorods with their SPRs at 685 and 560 nm (Figure 4d,f). The probability distributions of the bursts decay approximately exponentially with burst intensity. The extrapolation to a probability density of 10^{-4} of its maximum value provides a reliable and quantitative estimate of the maximum burst intensity, 500 and 200 counts/ms in Figure 4b,d, respectively.

Figure 5 shows measured maximum fluorescence enhancement factors for the 11 nanorods we studied under 594 nm (blue squares) and 633 nm (red squares) excitation. We compare our results with our theoretical estimations shown as open circles and dashed lines (blue: 594 nm and red: 633 nm excitation). Overall, our experimental results agree well with our theoretical predictions both for the maximum enhancement factors and for their dependence on the SPR wavelength.

Finally, we experimentally demonstrate decay rate enhancement by measuring the fluorescence lifetimes of enhanced and unenhanced CV molecules. Fluorescence lifetimes of enhanced CV molecules were measured by selecting the photons from fluorescence intensity bursts observed in a typical time trace, as shown in Figure 6a. The lifetime of unenhanced CV molecules was measured under similar experimental conditions but in the absence of nanorods. Figure 6b shows fluorescence decay histograms from unenhanced (purple) and enhanced CV molecules (from the bursts highlighted by red and green boxes in Figure 6a). The black curve is the instrument response function. The fluorescence of the enhanced CV molecules (red and green curves) decays clearly faster than that of the unenhanced CV molecules. The fluorescence decay of

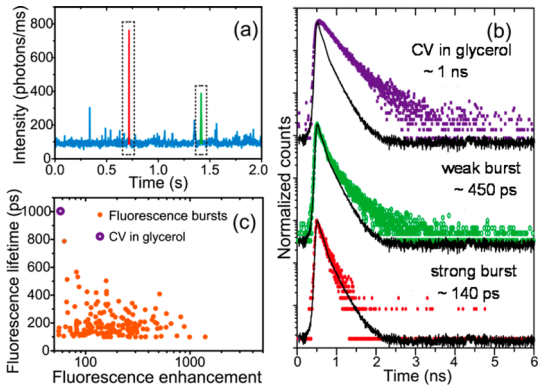

Figure 6. (a) Typical fluorescence time trace measured on a single gold nanorod using 635 nm picosecond pulsed laser excitation at an 80 MHz repetition rate. (b) Time-correlated single-photon histograms measured on unenhanced (top) and enhanced (middle, bottom) CV molecules during the bursts shown in (a). (c) Scatter plot of fluorescence lifetimes of enhanced CV molecules against the corresponding fluorescence enhancement factors.

unenhanced CV is well fitted by a single exponential with a lifetime of 1.0 ns. The decays of enhanced CV molecules (red and green curves) are nonexponential, with a short component well below our instrument resolution of ~120 ps. Longer components in the decay can be fitted with times of ~140 ps (red curve) and 450 ps (green curve). This clearly shows a shortening of the fluorescence lifetime of enhanced CV molecules by a factor of at least 7 compared to the unenhanced CV molecules. It is also interesting to note that Figure 6b also suggests that shorter fluorescence lifetimes are associated with higher enhancements.

To search for a correlation between fluorescence lifetime and fluorescence enhancement, we repeated the lifetime measurement on 200 fluorescence bursts. Figure 6c indeed shows a general correlation: higher enhancement is associated with shorter lifetime. However, we also find a significant population of bursts with weak fluorescence enhancement (less than 200 times) and shortened fluorescence lifetime (at least 7 times shorter than unenhanced CV). We speculate that these events are due to quenching of the fluorescence in close proximity to the metal. The quenching of fluorescence is expected to be the dominant factor when the distance between the gold nanorod and the CV molecule is less than 3 nm (Figure S2).

CONCLUSIONS

In this article we establish that, because of their narrow and intense plasmon resonance, wet-chemically synthesized gold nanorods are very efficient nanoantennas for enhancing the fluorescence of weak fluorophores. By selecting appropriate SPRs and excitation wavelengths, we show that fluorescence enhancement by a factor larger than 1000 is achievable. Such strong enhancement includes both the excitation rate enhancement and a significant enhancement of the decay rates of the emitter. Using DDA simulations, we estimate the excitation rate enhancement as 130 and the effective emission enhancement as 9, resulting in a total enhancement of 1100 induced by a gold nanorod with an SPR wavelength of 629 nm under 633 nm excitation for crystal violet molecules. We also demonstrate decay rate enhancement by directly measuring the fluorescence lifetime of enhanced CV molecules. Besides detecting individual weak fluorophores, an interesting application of such high fluorescence enhancement would be FCS at high concentrations of up to several μM.[38,39] This is particularly useful for studying many systems, notably biological ones, where the analyte concentration is comparatively high and cannot be reduced arbitrarily.

We note that the fluorescence enhancement by a chemically synthesized, single-crystalline gold nanorod antenna is comparable to that by lithographically made nanoantennas such as gold bowties. Indeed, the geometrical field enhancement (or lightning rod effect) of the bowtie antenna is much larger than that of the nanorod, whereas the plasmon resonance of the nanorod is much narrower and therefore more intense than the bowtie's resonance. Therefore, the nanorod antenna will be effective for a narrower range of wavelengths than the lithographically made bowtie antenna. This complementarity may be an advantage if selective enhancement of a specific dye is desired. In addition, the nanorod's plasmon resonance can be tuned easily from 600 nm to more than 1000 nm to match various dyes.

EXPERIMENTAL SECTION

We recently demonstrated strong enhancements by a gold nanorod for the fluorescence of weak emitters.[21] In this experiment, the fluorophores (crystal violet) were dissolved in a viscous solvent (glycerol) and slowly diffused through the near field of a gold nanorod that was immobilized on a glass coverslip.

Gold nanorods were synthesized by the seed-mediated growth method.[40] The average dimension of the nanorods was 25 nm × 60 nm. A typical scanning electron microscopy image is shown in Figure S5. The longitudinal surface plasmon resonance of these nanorods is approximately at 650 nm in water (Figure S5). Individual nanorods, coated with cetyltrimethylammonium bromide (CTAB), were isolated on a glass coverslip by spin coating from a water suspension. After spin coating, residual CTAB was removed by repeated washing with water and subsequent UV/ozone treatment for 30 min. Crystal violet (chemical structure shown in Figure S6) was used as the fluorophore. The absorption and emission maxima of CV are at 596 and 640 nm respectively (Figure 3b). Fluorescence enhancement experiments were performed on individual gold nanorods immersed in a 50 nM solution of CV in glycerol (Figure 3a) at room temperature. At that CV concentration, we estimate approximately 30 molecules in the focal volume at any

given time (considering a focal volume of 1 fL) and less than 0.001 molecule within the near-field volume of a nanorod.

Single-particle spectroscopy was performed on a home-built confocal microscope (Figure 3a). The details of the setup are described in previous reports.[35,41] In brief, a helium−neon laser (633 and 594 nm) and an Ar-ion laser (514 nm) are used as excitation sources. Circular polarization was used, as it excites the flat-lying nanorods irrespective of their orientation in the focal plane. An oil immersion objective with a numerical aperture of 1.25 was used to focus the excitation laser to a diffraction-limited spot of approximately 300 nm in diameter (Figure 1a). The luminescence signal was separated from the excitation laser using appropriate notch filters (removing 633, 594, or 514 nm light depending on the excitation wavelength) and detected either by avalanche photodiodes or by a liquid-nitrogen-cooled CCD spectrometer. Images were constructed by scanning the sample across the laser focus using a XYZ piezoscanner.

Fluorescence lifetimes of CV molecules were measured using a time-correlated single-photon counting setup (Pico-Quant). A 635 nm pulsed laser (~100 ps pulse width) was used as excitation source. An avalanche photodiode (MPD) was used as detector. Using NIM timing output from the MPD, we could improve the instrument response function to ~120 ps.

Conflict of Interest: The authors declare no competing financial interest.

Acknowledgment. S.K., H.Y., and M.O. acknowledge financial support from the ERC Advanced Grant SiMoSoMa. S.K. and P.Z. acknowledge financial support from The Netherlands Organization for Scientific Research (ECHO and Veni Fellowship, respectively). P.M.R.P. acknowledges financial support from Fundação para a Ciência e a Tecnologia (Ciência 2008 and PTDC/CTM-NAN/2700/2012).

Supporting Information Available: Figures S1−S10 and the theoretical description of fluorescence enhancement are available free of charge *via* the Internet at http://pubs.acs.org.

REFERENCES AND NOTES

1. Moerner, W. E.; Orrit, M. Illuminating Single Molecules in Condensed Matter. *Science* **1999**, *283*, 1670–1676.
2. Zondervan, R.; Kulzer, F.; Berkhout, G. C. G.; Orrit, M. Local Viscosity of Supercooled Glycerol near T-G Probed by Rotational Diffusion of Ensembles and Single Dye Molecules. *Proc. Natl. Acad. Sci. U.S.A.* **2007**, *104*, 12628–12633.
3. Mackowiak, S. A.; Herman, T. K.; Kaufman, L. J. Spatial and Temporal Heterogeneity in Supercooled Glycerol: Evidence from Wide Field Single Molecule Imaging. *J. Chem. Phys.* **2009**, *131*, 14.
4. Huang, B.; Bates, M.; Zhuang, X. W. Super-Resolution Fluorescence Microscopy. *Annu. Rev. Biochem.* **2009**, *78*, 993–1016.
5. Xie, X. S.; Lu, H. P. Single-Molecule Enzymology. *J. Biol. Chem.* **1999**, *274*, 15967–15970.
6. Velonia, K.; Flomenbom, O.; Loos, D.; Masuo, S.; Cotlet, M.; Engelborghs, Y.; Hofkens, J.; Rowan, A. E.; Klafter, J.; Nolte, R. J. M.; *et al*. Single-Enzyme Kinetics of CALB-Catalyzed Hydrolysis. *Angew. Chem., Int. Ed.* **2005**, *44*, 560–564.
7. Ming, T.; Chen, H. J.; Jiang, R. B.; Li, Q.; Wang, J. F. Plasmon-Controlled Fluorescence: Beyond the Intensity Enhancement. *J. Phys. Chem. Lett.* **2012**, *3*, 191–202.
8. Lakowicz, J. R. Plasmonics in Biology and Plasmon-Controlled Fluorescence. *Plasmonics* **2006**, *1*, 5–33.
9. Tam, F.; Goodrich, G. P.; Johnson, B. R.; Halas, N. J. Plasmonic Enhancement of Molecular Fluorescence. *Nano Lett.* **2007**, *7*, 496–501.
10. Munechika, K.; Chen, Y.; Tillack, A. F.; Kulkarni, A. P.; Plante, I. J. L.; Munro, A. M.; Ginger, D. S. Spectral Control of Plasmonic Emission Enhancement from Quantum Dots near Single Silver Nanoprisms. *Nano Lett.* **2010**, *10*, 2598–2603.
11. Bharadwaj, P.; Anger, P.; Novotny, L. Nanoplasmonic Enhancement of Single-Molecule Fluorescence. *Nanotechnology* **2007**, 18.
12. Mertens, H.; Koenderink, A. F.; Polman, A. Plasmon-Enhanced Luminescence near Noble-Metal Nanospheres: Comparison of Exact Theory and an Improved Gersten and Nitzan Model. *Phys. Rev. B* **2007**, *76*.
13. Mertens, H.; Polman, A. Strong Luminescence Quantum-Efficiency Enhancement near Prolate Metal Nanoparticles: Dipolar *versus* Higher-Order Modes. *J. Appl. Phys.* **2009**, *105*.
14. Kühn, S.; Håkanson, U.; Rogobete, L.; Sandoghdar, V. Enhancement of Single-Molecule Fluorescence Using a Gold Nanoparticle as an Optical Nanoantenna. *Phys. Rev. Lett.* **2006**, *97*, 017402.
15. Anger, P.; Bharadwaj, P.; Novotny, L. Enhancement and Quenching of Single-Molecule Fluorescence. *Phys. Rev. Lett.* **2006**, *96*, 113002.
16. Kinkhabwala, A.; Yu, Z. F.; Fan, S. H.; Avlasevich, Y.; Müllen, K.; Moerner, W. E. Large Single-Molecule Fluorescence Enhancements Produced by a Bowtie Nanoantenna. *Nat. Photonics* **2009**, *3*, 654–657.
17. Farahani, J. N.; Pohl, D. W.; Eisler, H. J.; Hecht, B. Single Quantum Dot Coupled to a Scanning Optical Antenna: A Tunable Superemitter. *Phys. Rev. Lett.* **2005**, *95*, 017402.
18. Curto, A. G.; Volpe, G.; Taminiau, T. H.; Kreuzer, M. P.; Quidant, R.; van Hulst, N. F. Unidirectional Emission of a Quantum Dot Coupled to a Nanoantenna. *Science* **2010**, *329*, 930–933.
19. Aouani, H.; Mahboub, O.; Bonod, N.; Devaux, E.; Popov, E.; Rigneault, H.; Ebbesen, T. W.; Wenger, J. Bright Unidirectional Fluorescence Emission of Molecules in a Nanoaperture with Plasmonic Corrugations. *Nano Lett.* **2011**, *11*, 637–644.
20. Habteyes, T. G.; Dhuey, S.; Wood, E.; Gargas, D.; Cabrini, S.; Schuck, P. J.; Alivisatos, A. P.; Leone, S. R. Metallic Adhesion Layer Induced Plasmon Damping and Molecular Linker as a Nondamping Alternative. *ACS Nano* **2012**, *6*, 5702–5709.
21. Yuan, H.; Khatua, S.; Zijlstra, P.; Yorulmaz, M.; Orrit, M. Thousand-Fold Enhancement of Single-Molecule Fluorescence near a Single Gold Nanorod. *Angew. Chem., Int. Ed.* **2013**, *52*, 1217–1221.
22. Vigderman, L.; Khanal, B. P.; Zubarev, E. R. Functional Gold Nanorods: Synthesis, Self-Assembly, and Sensing Applications. *Adv. Mater.* **2012**, *24*, 4811–4841.
23. Ye, X. C.; Zheng, C.; Chen, J.; Gao, Y. Z.; Murray, C. B. Using Binary Surfactant Mixtures to Simultaneously Improve the Dimensional Tunability and Monodispersity in the Seeded Growth of Gold Nanorods. *Nano Lett.* **2013**, *13*, 765–771.
24. Grabinski, C.; Schaeublin, N.; Wijaya, A.; D'Couto, H.; Baxamusa, S. H.; Hamad-Schifferli, K.; Hussain, S. M. Effect of Gold Nanorod Surface Chemistry on Cellular Response. *ACS Nano* **2011**, *5*, 2870–2879.
25. van den Broek, B.; Ashcroft, B.; Oosterkamp, T. H.; van Noort, J. Parallel Nanometric 3d Tracking of Intracellular Gold Nanorods Using Multifocal Two-Photon Microscopy. *Nano Lett.* **2013**, *13*, 980–986.
26. Lu, G. W.; Zhang, T. Y.; Li, W. Q.; Hou, L.; Liu, J.; Gong, Q. H. Single-Molecule Spontaneous Emission in the Vicinity of an Individual Gold Nanorod. *J. Phys. Chem. C* **2011**, *115*, 15822–15828.
27. Mohammadi, A.; Sandoghdar, V.; Agio, M. Gold Nanorods and Nanospheroids for Enhancing Spontaneous Emission. *New J. Phys.* **2008**, *10*, 105015.
28. Brey, L. A.; Schuster, G. B.; Drickamer, H. G. High-Pressure Studies of Effect of Viscosity on Fluorescence Efficiency in Crystal Violet and Auramine O. *J. Chem. Phys.* **1977**, *67*, 2648–2650.
29. Johnson, P. B.; Christy, R. W. Optical Constants of Noble Metals. *Phys. Rev. B* **1972**, *6*, 4370–4379.
30. D'Agostino, S.; Della Sala, F.; Andreani, L. C. Dipole-Excited Surface Plasmons in Metallic Nanoparticles: Engineering Decay Dynamics within the Discrete-Dipole Approximation. *Phys. Rev. B* **2013**, *87*, 205413.
31. Jackson, J. D. *Classical Elctrodynamics*, 3rd ed.; John Wiley & Sons, Inc: New York, 1999; p 411.
32. Zuloaga, J.; Prodan, E.; Nordlander, P. Quantum Description of the Plasmon Resonances of a Nanoparticle Dimer. *Nano Lett.* **2009**, *9*, 887–891.

33. Zuloaga, J.; Nordlander, P. On the Energy Shift between near-Field and Far-Field Peak Intensities in Localized Plasmon Systems. *Nano Lett.* **2011**, *11*, 1280–1283.
34. Aizpura, J.; Esteban, R. *Optical Antennas*; Cambridge University Press: United Kingdom, 2013; Chapter 5, pp 64−80.
35. Yorulmaz, M.; Khatua, S.; Zijlstra, P.; Gaiduk, A.; Orrit, M. Luminescence Quantum Yield of Single Gold Nanorods. *Nano Lett.* **2012**, *12*, 4385–4391.
36. Slaughter, L. S.; Wu, Y. P.; Willingham, B. A.; Nordlander, P.; Link, S. Effects of Symmetry Breaking and Conductive Contact on the Plasmon Coupling in Gold Nanorod Dimers. *ACS Nano* **2010**, *4*, 4657–4666.
37. Funston, A. M.; Novo, C.; Davis, T. J.; Mulvaney, P. Plasmon Coupling of Gold Nanorods at Short Distances and in Different Geometries. *Nano Lett.* **2009**, *9*, 1651–1658.
38. Kinkhabwala, A. A.; Yu, Z. F.; Fan, S. H.; Moerner, W. E. Fluorescence Correlation Spectroscopy at High Concentrations Using Gold Bowtie Nanoantennas. *Chem. Phys.* **2012**, *406*, 3–8.
39. Estrada, L. C.; Aramendia, P. F.; Martinez, O. E. 10000 Times Volume Reduction for Fluorescence Correlation Spectroscopy Using Nano-Antennas. *Opt. Express* **2008**, *16*, 20597–20602.
40. Nikoobakht, B.; El-Sayed, M. A. Preparation and Growth Mechanism of Gold Nanorods (Nrs) Using Seed-Mediated Growth Method. *Chem. Mater.* **2003**, *15*, 1957–1962.
41. Gaiduk, A.; Ruijgrok, P. V.; Yorulmaz, M.; Orrit, M. Detection Limits in Photothermal Microscopy. *Chem. Sci.* **2010**, *1*, 343–350.